International Journal of Scientific Engineering and Applied Science (IJSEAS) – Volume-7, Issue-10, October 2021
ISSN: 2395-3470
www.ijseas.com

Analytical Modelling and Computer Simulation Of Effective Engineering Properties Of Sandwich Composite Panels Using Axial-Compressive And Flexural Techniques

Umar Farooq[*1], Peter Myler[2], Mamoona Siddique[3]

[1, 2]Faculty of Engineering, Support and Advanced Sciences, University of Bolton, BL3 5AB, United Kingdom

Email: U.Farooq@bolton.ac.uk, pm8@bolton.ac.uk

[3]Lecturer, Department of Mathematics, Government Degree College for Women, Sargodha 4000 Pakistan.

Email: monamaths0@gmail.com

Corresponding author: Umar Farooq[*1], Email: adalzai3@yahoo.co.uk

Abstract

This work describes analytical formulation and computer simulation to approximate effective engineering properties of sandwich composite panels. The sandwich composite structures are composed of thin, stiff face-sheets bonded to a relatively thick lightweight core in between. Such structures demonstrate high strength and stiffness potential to weight ratios and energy absorption capacity in many aerospace engineering applications. Nonetheless, the structures are influence by detrimental dynamic behaviour of aircraft during service life that may be threat to human life and structural integrity. Thus, to ensure the reliable and safe performance of aircrafts dire need exists to study and better understand engineering properties of sandwich structures at pre-design stage to avert the detrimental threats. Majority of the existing studies consist of routine experimental testing to ascertain engineering properties on ad-hoc basis to improve performance capability without addition weight penalty. A very few analytical and simulation studies can be found in the area due to the complexity involved with mathematical modelling of mechanical properties of the sandwich panels. Current work is based on developing analytical formulation and computer simulation of the effective properties using MATLAB^{TM} software. Subsequently, the simulation generated quantities were validated against the benchmark data results available in the literature and found to be in good agreement. Findings have established suitability of the simulation for the engineering properties. The proposed study is a positive effort to supplement the existing studies in the field. The study may be easily modified and utilized to approximate engineering properties of similar panels and use them to accommodate stiffness.

Key Words: Sandwich Structures; Aluminium Foam Core; CFRP skins; Axial-Compression; Flexural Bending; Mechanical Properties

1 Introduction

Sandwich structures consist of stiff and strong skins front and rear panels separated by a light weight core in between [1]. They posses high strength-to-weight and stiffness-to-weight ratios, energy absorption characteristics, capability of multifunctional design, good vibration reduction, relatively low cost, and stress wave attenuation [2]. Owing to the superior properties sandwich structures being widely used in aerospace and maritime, civil and military, medical and sporting goods.

During service life an aircraft may influence by dynamics of overall body structures that can be detrimental to its integrity. Therefore, investigations are needed at pre-design stage for reliable mechanical properties to be used to build safe and efficient sandwich structures [3]. Majority of the previous studies are experimental, and relevant ones are selected to refer below. The mechanical property evaluations are studied following standard test method for tensile properties of polymer matrix composite materials [4], [5] for sandwich composite structures. Characterization of syntactic foams and metal matrix syntactic foam core and their sandwich composites suggested using a 3–point bending tests [6]. The crack propagation was investigated through the alumina particles for failed specimens instead of interfacial failure. Axial-compressive properties of polymer matrix composite materials with unsupported gage section by shear loading were investigated in [7]. In-plane shear response of polymer matrix composite materials by tensile test of a 45 laminate is reported in [8]. Axial-compressive strength and energy absorption of sandwich panels with Aluminium foam-filled corrugated cores were studied in [9]. It was noted that shear deformation might result in disintegration of joint structure leading to catastrophic failures during future operations [10].

The facings are loaded primarily in tension or compression to resist flexural while the core made up of lightweight and soft material resists the shear stresses are reported in [11]. Engineering properties using three-point flexural tests of sandwich beams with aluminium foam-filled corrugated cores were carried out in [12]. The equivalent flexural rigidity properties of sandwich composite panels were analysed in [13]. Shear characterization of sandwich core material properties using four-point flexural are detailed in [14]. Insight into the shear behaviour of composite sandwich panels with foam core can be seen in [15].

Study on axial-compressive properties of syntactic foams for marine applications using three-point flexural tests of sandwich structures were performed in [16]. Studies of foam density

variations in composite sandwich panels under high velocity impact loading were conducted in [17], [18]. Engineering properties were utilized of metal and polymeric foam sandwich plates under low velocity impact to investigate relative performance in [19]. An investigation on the flexural properties of balsa and polymer foam core sandwich structures reported influence of core type and contour in [20].

Engineering properties of composite sandwich panels with cores made of aluminium honeycomb and foam investigated the effects of different types of core materials on the failure mechanisms under four-point bend flexural tests in [21]. They concluded that the yield stress of the core material was a key parameter in controlling the failure mechanism of the sandwich structure in the further study [22]. The effect of different types of core material engineering properties on the flexural behaviour of sandwich composites was investigated in [23]. Engineering properties to study damage characteristics analysis of GFRP-balsa sandwich beams under four-point fatigue flexural were carried out in [24]. Three-point flexural deflection and failure mechanism map of sandwich beams with second-order hierarchical corrugated truss core was conducted in [25].

Scaling effects in the mechanical response of sandwich structures based on corrugated composite core properties are reported in [26]. Engineering properties of single- and double-layer aluminium corrugated core sandwiches were determined under quasi-static and dynamic loadings in [27]. Modelling of axial and shear stresses in multilayer sandwich beams with stiff core layers properties are presented in [28]. Improvement of the mechanical performance of the perforated foam core sandwich composites by stitching was experienced in [29]. Effective engineering properties were used to study performance failure analyses of adhesively bonded steel corrugated sandwich structures under transverse, transverse shear strength, load resistance, and energy absorption under three-point flexural test [30].

Honeycomb–corrugation hybrid as a novel sandwich core for significantly enhanced axial-compressive performance according to [31]. Experimental and numerical investigation of skin/lattice stiffener debonding growth in composite panels under flexural loading can be found in [32]. Numerical analysis of flexural strengthening of timber beams reinforced with CFRP strips are given in [33]. Analytical investigation of perforation of aluminium–foam sandwich panels under ballistic impact can be seen in [34]. Analytical study of high velocity impact on sandwich panels with foam core and Aluminium face-sheets are reported in [35], [36]. A numerical analysis approach for evaluating elastic constants of sandwich structures

with various cores is presented in [37]. Experimental and numerical investigation of a blunt rigid projectile penetrating into a sandwich panel having aluminium foam core have been investigated in [38]. A numerical study engineering properties on the impact behaviour of foam-cored cylindrical sandwich shells subjected to normal and oblique impacts are described in [39], [40]. Many research studies have explored new types of sandwich structures by changing the type, density, and engineering properties of the material used for the core [41]. The study demonstrated that deformation and failure characteristics of the foam core play a very important role in determining the mechanical performance of the sandwich structure.

Experimental and numerical research on the low velocity impact behaviour of hybrid corrugated core sandwich structure properties was investigated in [42]. Effect of the skin thickness, core densities, and indenter shape on the impact behaviour and failure mechanisms of engineering properties of sandwich structures have also been described.

A very few analytical studies are available on the topic because of the complexity of mathematical equations that govern properties of sandwich structures. However, experiments are time and resources consuming and require ancillaries which can be avoided by using computer simulations. The engineering property information is very important in order to use the materials as core and skins in sandwich composite systems. The computer simulations can efficiently predict energy absorption and peak loads for a variety of combinations of materials and geometry by considering competing mechanisms. On the basis of conducted analyses, it can be concluded that engineering properties of this type of materials may also be computed efficiently, reliably, and economically.

2 Materials and methods

2.1 Equivalent plate transformation

A sandwich panel of length a, width b and thickness $h_0 = H$ is referred to a Cartesian co-ordinate system $x_1, x_2, x_3 (0 \leq x_1 \leq W, 0 \leq x_2 \leq b, -H/2 \leq x_3 \leq H/2)$ and assumed to be symmetric with respect to the mid-plane $x_3 = 0$, with the face thickness h_f and the core thickness $H_I = 2h_c$. The length of the plates are set to 5 m, the width to 3 m and the height to 0.27 m. They are subjected to a uniformly distributed load (3 kN/m^2) and are simply supported on four edges. The plates are free to expand/retract in x- and y-direction along two sides. The boundary condition is assigned a width of 5 centimetres when using solid elements to ensure a good transfer of the support force to the three layers without the risk of local

distortion corrupting the result. A linear boundary condition is used for the shell elements. The transformation is executed in two steps, see **Figure 1**.The first step transforms the sandwich structure to a three layered plate and the second part translates the three layers into one layer. The first transformation is mainly done by loading the structure in different ways and measuring displacements. The equivalent stiffness of the cores are then obtained from simple formulas that treat shear and flexural deflection. The second transformation, however, is derived analytically from assumptions regarding the behaviour and equilibrium of a three layered sandwich plate.

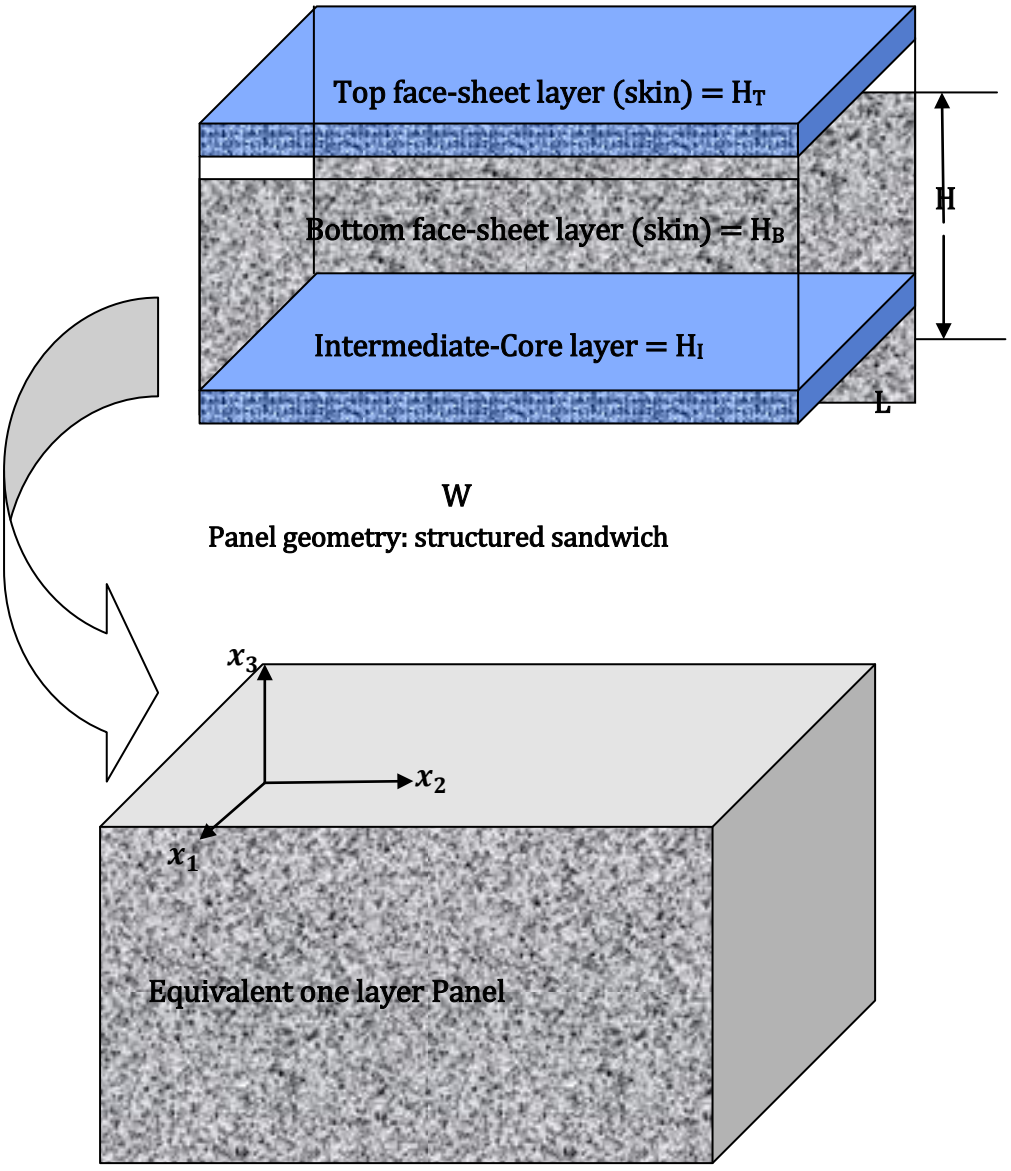

Figure 1: Illustration of the two steps in the transformation between a structured sandwich plate to an equivalent one layered plate.

Generally, the top and bottom face sheets are assigned stiffer properties compared to the core. Engineering constants for top-layer, core-layer, and bottom-layer properties consisting of Young's (elastic) moduli, three Poisson's ratios, and three shear moduli are given in **Table 1**, **Table 2**, and **Table 3**, respectively. These properties are chosen from [3], a total of 7 sets of material properties having different parameters are presented. The last two material sets have a stiffer core compared to the face sheets. This is not a realistic case and is chosen only on the basis to study and understand the behaviour of the different transformations better. To ensure that the chosen materials have a realistic behaviour, a check of the load-deflection verification analysis is performed.

Table 1: Top-layer mechanical properties sets 1-7

Five sets have stiffer face sheets								
E_{xx}	E_{yy}	E_{zz}	ν_{xx}	ν_{yy}	ν_{zz}	G_{12}	G_{13}	G_{23}
100.6e9	20.e9	20.e9	0.2	0.3	0.1	5e9	10e9	7e9
210.6e9	210.6e9	210.6e9	0.3	0.3	0.3	80.7e9	80.7e9	80.7e9
100.6e9	20.e9	20.e9	0.2	0.3	0.1	5e9	10e9	7e9
2000.6e9	1000e9	500.e9	0.05	0.06	0.05	200e9	100e9	400e9
206e9	2e9	50.e9	0.15	0.26	0.12	5e9	3e9	1e9
Two sets have a weaker face sheets compared to the core								
2e9	5e9	10e9	0.2	0.1	0.3	5e9	0.3e9	0.1e9
0.2e9	5e9	0.3e9	0.12	0.11	0.23	0.05e9	0.03e9	0.01e9

Table 2: Core-layer mechanical properties sets 1-7

Five sets have stiffer face sheets								
E_{xx}	E_{yy}	E_{zz}	ν_{xx}	ν_{yy}	ν_{zz}	G_{12}	G_{13}	G_{23}
2e9	0.2e9	0.2e9	0.1	0.2	0.1	0.1e9	0.5e9	0.3e9
0.36e9	0.36e9	0.36e9	0.08	0.08	0.08	0.097e9	0.097e9	0.097e9
2e9	0.2e9	0.2e9	0.1	0.2	0.1	0.1e9	0.5e9	0.3e9
0.02e9	0.04e9	0.5e9	0.1	0.1	0.05	0.5e9	0.9e9	01e9
0.02e9	0.046e9	0.2e9	0.13	0.22	0.09	0.4e9	0.09e9	0.1e9
Two sets have a stiffer core compared to the face sheets								
200e9	100e9	300e9	0.23	0.12	0.3	10e9	0.5e9	2e9
200e9	1000e9	600e9	0.15	0.12	0.23	100e9	6e9	10e9

Table 3: Bottom-layer mechanical properties sets 1-7

Five sets have stiffer face sheets								
E_{xx}	E_{yy}	E_{zz}	ν_{xx}	ν_{yy}	ν_{zz}	G_{12}	G_{13}	G_{23}
210.4e9	210.4e9	210.4e9	0.3	.3	0.3	80.7e9	80.7e9	80.7e9
20.4e9	100.4e9	100.4e9	0.3	.31	0.29	10.e9	5e9	7e9
20.4e9	100.4e9	100.4e9	0.3	.31	0.29	10.e9	5e9	7e9
400e9	200e9	40e9	0.1	.1	0.29	50.e9	53e9	71e9
15e9	40e9	1e9	0.15	.11	0.15	2.e9	3e9	24e9
Two sets have a weaker face sheets compared to the core								
10e9	20e9	2e9	0.12	.15	0.2	5e9	1e9	5e9
1e9	2e9	22e9	0.17	.14	0.15	0.5e9	10e9	1e9

2.2 Derivations of equivalent properties of a three layered sandwich structure

The transformation is performed for nine deferent elastic parameters, three Young's modulus, three shear modulus and three Poisson's ratio. No interaction between the different parameters is assumed. There are two different investigated approaches when transforming the elastic moduli E_{11} and E_{22}, see figure 3.1.1, either assume a constant modulus based on axial loaded deformation [1], or constant flexural rigidity. It is not apparent which of these base assumptions simulate the reality best, consequently both variations have to be investigated further in an extensive verification.

The assumptions regarding the transformation of the elastic modulus in z-direction is only compression because of the low height to length ratio. This means that there is no flexural in this direction, thus the transformation is only based on the assumption of axial loaded deformation for both methods.

2.2.1 Equivalent axial-compressive modulus

For determining the in-plane Young's modulus E_{11} and E_{22}, the following setup of the plate and loading is used as depicted in **Figure 2** based on [1].

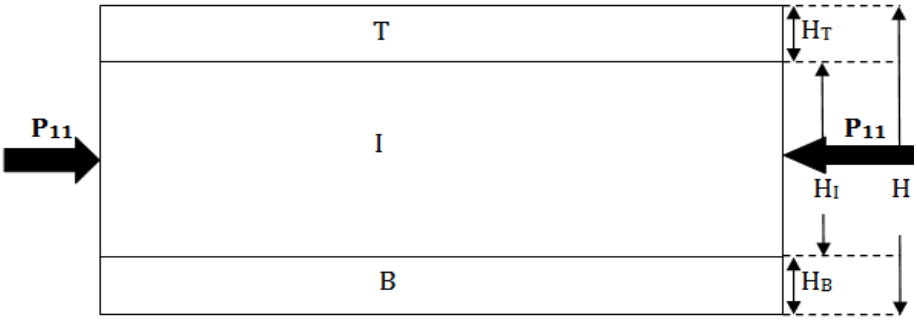

Figure 2: Assumed load in x-direction and y-direction for transformation based on axial loaded (distributed over all layers) deformation

Assume loading of the plate in x-direction (direction 1) and that the load is divided to all layers, see fig.. where T-top layer, I-interface layer, B-bottom layer:

$$P_{11} = P_{11}^{T} + P_{11}^{I} + P_{11}^{B} \quad \textbf{(1)}$$

Which is the same as:

$$\sigma_{11}.A_{11} = \sigma_{11}^{T}.A_{11}^{T} + \sigma_{11}^{I}.A_{11}^{I} + \sigma_{11}^{B}.A_{11}^{B} \quad \textbf{(2)}$$

That can be rewritten as,

$$\sigma_{11} = \sigma_{11}^{T}.\frac{A_{11}^{T}}{A_{11}} + \sigma_{11}^{I}.\frac{A_{11}^{I}}{A_{11}} + \sigma_{11}^{\boldsymbol{B}}.\frac{A_{11}^{B}}{A_{11}} \quad \textbf{(3)}$$

Where area elements are,

$$A_{11} = H.W, A_{11}^{T} = H^{T}.W \ , A_{11}^{I} = H^{I}.W \ , \ A_{11}^{B} = H^{B}.W \quad \textbf{(4)}$$

Let

$$\alpha_T = \frac{H_T}{H}, \alpha_I = \frac{H_I}{H}, \alpha_B = \frac{H_B}{H} \quad \textbf{(5)}$$

Substitute (5) and (4) into (3), simplify and receive:

$$\sigma_{11} = \sigma_{11}^{T}.\alpha_T + \sigma_{11}^{I}.\alpha_{\mathrm{I}} + \sigma_{11}^{B}.\alpha_B \quad \textbf{(6)}$$

Divide equation (6) by ε_{11}:

$$\frac{\sigma_{11}}{\varepsilon_{11}} = \frac{\sigma_{11}^{T}}{\varepsilon_{11}}.\alpha_T + \frac{\sigma_{11}^{I}}{\varepsilon_{11}}.\alpha_I + \frac{\sigma_{11}^{B}}{\varepsilon_{11}}.\alpha_B \quad \textbf{(7)}$$

Which gives the transformation of E_{11} based on axial loaded deformation:

$$E_{11} = E_{11}^{T}.\alpha_T + E_{11}^{I}.\alpha_{\mathrm{I}} + E_{11}^{B}.\alpha_B \quad \textbf{(8)}$$

The same procedure can be used to determine E_{22}

$$E_{22} = E_{22}^{T}.\alpha_T + E_{22}^{I}.\alpha_{\mathrm{I}} + E_{22}^{B}.\alpha_B \quad \textbf{(9)}$$

2.2.2 Equivalent constants-flexural method

The computation of the equivalent moduli of E_{11} and E_{22} for the flexural method is based on flexural stiffness. The following procedure is based on the setup, which can be seen in **Figure 3**. The flexural stiffness of the plate is treated as a sandwich composite beam, which simplifies the theoretical analysis. In order to formulate level position of the neutral axis, the following procedure has to be followed.

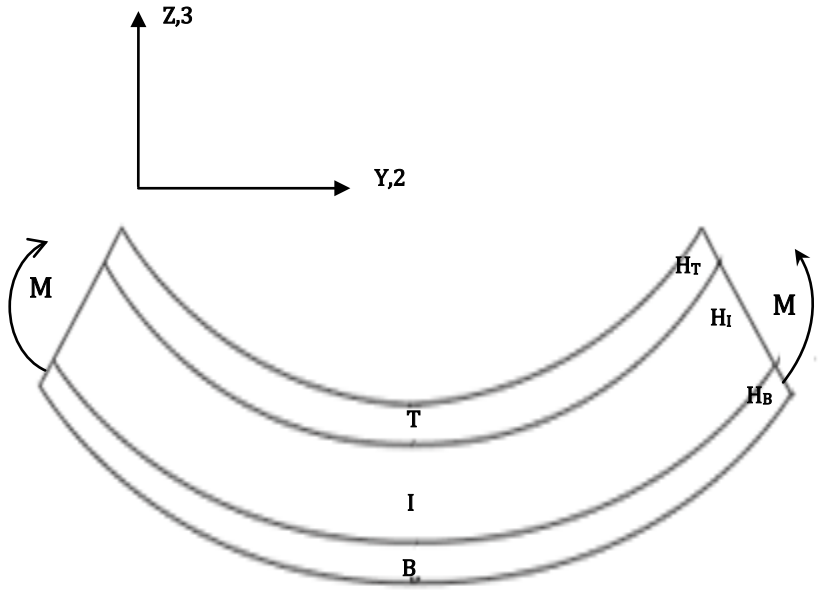

Figure 3: Assumed load and deflection for the transformation based on flexural rigidity

Consider a three layered sandwich structure, see **Figure 4**. In order to calculate at shifted level the neutral axis situated, the following procedure has to be performed.

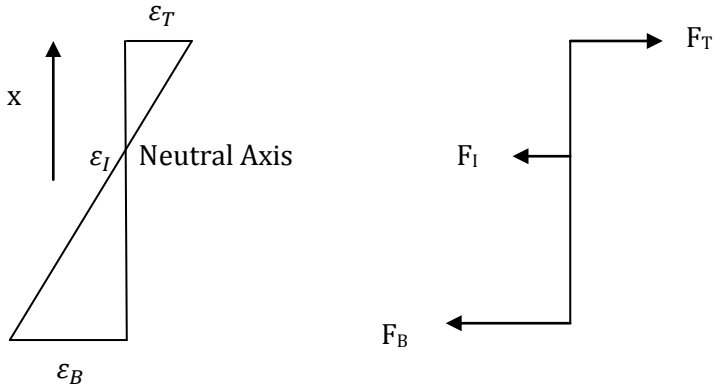

Figure 4 : Strain and fore equilibrium

To establish the relation between the different strains of the three layers, where H is the total of the sandwich plate and W is the width:

$$\frac{\varepsilon_T}{x-\frac{H_T}{2}} = \frac{\varepsilon_B}{x-H+\frac{H_B}{2}} \Longrightarrow \varepsilon_B = \frac{\varepsilon_B\left(x-H+\frac{H_B}{2}\right)}{x-\frac{H_T}{2}},\ \varepsilon_I = \frac{\varepsilon_T\left(x-\frac{H}{2}\right)}{x-\frac{H_T}{2}} \qquad \textbf{(10)}$$

Establish the global equilibrium and rewriting:

$$F_T + F_I + F_B = 0 \Longrightarrow (\varepsilon.E.A)_T + (\varepsilon.E.A)_I + (\varepsilon.E.A)_B = 0 \quad \textbf{(11)}$$

Insert equation (11) and (12) into equation (14) gives:

$$\varepsilon_T.E_T.A_T + \frac{\varepsilon_T\left(x-\frac{H}{2}\right)}{x-\frac{H_T}{2}}.E_T.A_T + \frac{\varepsilon_T\left(x-H+\frac{H_B}{2}\right)}{x-\frac{H_T}{2}}.E_B.A_B = 0 \quad \textbf{(12)}$$

Solve this equation for x and receive:

$$x = \frac{-E_B H_B^2 + 2E_B H H_B + E_T H_T^2 + E_I H H_I}{2(E_B H_B + E_I H_I + E_T H_T)} \quad \textbf{(13)}$$

Assuming that the flexural rigidity of the plate will stay constant yields following expression:

$$D = D_T + D_I + D_B \quad \textbf{(14)}$$

Where $D_T, D_I \; and \; D_B$ as:

$D_T = E_{11}^T.\frac{I_{11}^T}{W}$ and $I_{11}^T = W.\frac{H_T^3}{12} + W.H_T.x^2$ so

$$D_T = E_{11}^T\left(\frac{H_T^3}{12} + H_T.x^2\right), D_I = E_{11}^I\left(\frac{H_I^3}{12} + H_I\left(x - \frac{H_T}{2} - x^2\right)^2\right) \quad \textbf{(15)}$$

$$D_B = E_{11}^B\left(\frac{H_B^3}{12} + H_B(H-x)^2\right) \quad \textbf{(16)}$$

The single layer stiffness: $D = E_{EQ}.\frac{H^3}{12}$ **(17)**

Using equations (11), (16) and (17) in (12), the elastic modulus (E_{EQ}) based on flexural rigidity can be expressed:

$$E_{EQ} = \frac{12E_T\left(\frac{H_T^3}{12} + \frac{H_T\left(-E_B H_B^2 + 2E_B H H_B + E_T H_T^2 + E_I H H_I\right)^2}{4\left(E_B H_B + E_I H_I + E_T H_T\right)^2}\right)}{H^3}$$

$$+ \frac{12E_B\left(\frac{H_B^3}{12} + H_B\left(\frac{H - E_B H_B^2 + 2E_B H H_B + E_T H_T^2 + E_I H H_I}{2E_B H_B + 2E_I H_I + 2E_T H_T}\right)^2\right)}{H^3}$$

$$+ \frac{12E_I\left(\frac{H_I^3}{12} + H_I\left(\frac{H_I}{2} + \frac{H_T}{2} - \frac{-E_B H_B^2 + 2E_B H H_B + E_T H_T^2 + E_I H H_I}{2E_B H_B + 2E_I H_I + 2E_T H_T}\right)^2\right)}{H^3} \quad \textbf{(18)}$$

Equation (18) can be used to express both E_{11} and E_{22}.

2.2.3 Equivalent elastic constants in z-direction

The equivalent elastic engineering modulus in z-direction can be described as compression of the plate over its thickness. This process is also used in both transformational methods, axial-compressive and flexural derived from [1].

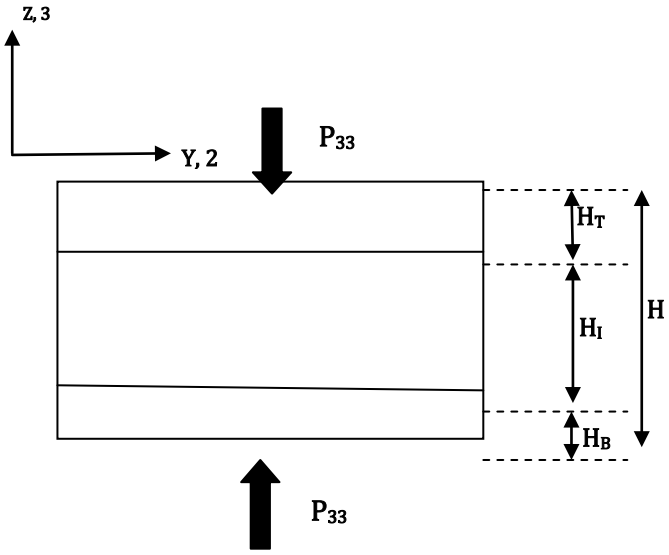

Figure 5: Assumed load in z-direction evenly distributed over the face sheet.

Assume load in z-direction (direction 3), see fig--. The force P_{33} is distributed over the whole bottom an top face sheets:

$$\sigma_{33} = \frac{P_{33}}{A_{33}} \quad \textbf{(19)}$$

All stresses must be transformed to all layers of the plate, which leads to

$$\sigma_{33} = \sigma_{33}^{T} + \sigma_{33}^{I} + \sigma_{33}^{B} \quad \textbf{(20)}$$

The strains of each layer can be expresses as:

$$\varepsilon_{33}^{T} = \frac{\sigma_{33}^{T}}{E_{33}^{T}}, \varepsilon_{33}^{I} = \frac{\sigma_{33}^{I}}{E_{33}^{I}}, \varepsilon_{33}^{B} = \frac{\sigma_{33}^{B}}{E_{33}^{B}} \quad \textbf{(21)}$$

The total displacement can be expressed by the sum of the contribution from all layers

$$\delta_{33} = \delta_{33}^{T} + \delta_{33}^{I} + \delta_{33}^{B} = \varepsilon_{33}^{T}.H^{T} + \varepsilon_{33}^{I}.H^{I} + \varepsilon_{33}^{B}.H^{B} \quad \textbf{(22)}$$

$$\varepsilon_{33} = \frac{\delta_{33}}{H} = \frac{\varepsilon_{33.H}^{T}T}{H} + \frac{\varepsilon_{33.H}^{I}I}{H} + \frac{\varepsilon_{33.H}^{B}B}{H} \quad \textbf{(23)}$$

Divide equation (23) by σ_{33} and acquire and applicate

$$\frac{\varepsilon_{33}}{\sigma_{33}} = \frac{\varepsilon^{T}_{33.\alpha T}}{\sigma_{33}} + \frac{\varepsilon^{I}_{33.\alpha I}}{\sigma_{33}} + \frac{\varepsilon^{B}_{33.\alpha B}}{\sigma_{33}} \quad \textbf{(24)}$$

Solve for E_{33} to get the equation for the transformation of the elastic modulus in z-direction:

$$\frac{1}{E_{33}} = \frac{\alpha^{T}}{E^{T}_{33}} + \frac{\alpha^{I}}{E^{I}_{33}} + \frac{\alpha^{B}}{E^{B}_{33}} \Longrightarrow E_{33} = \frac{1}{\frac{\alpha^{T}}{E^{T}_{33}} + \frac{\alpha^{I}}{E^{I}_{33}} + \frac{\alpha^{B}}{E^{B}_{33}}} \quad \textbf{(25)}$$

2.2.4 Equivalent shear moduli

This section treats the calculation of the equivalent shear moduli, the expressions are obtained for both the axial-compressive and flexural methods [1].

The shear stiffness G_{12} is obtained by summation of the stiffness of the individual, see **Figure 6**, layers in the same manner as for E_{11}calculated from the axial loaded deflection. The equation for transformation will therefore become:

$$G_{12} = G^{T}_{12}.\alpha^{T} + G^{I}_{12}.\alpha^{I} + G^{B}_{12}.\alpha^{B} \quad \textbf{(26)}$$

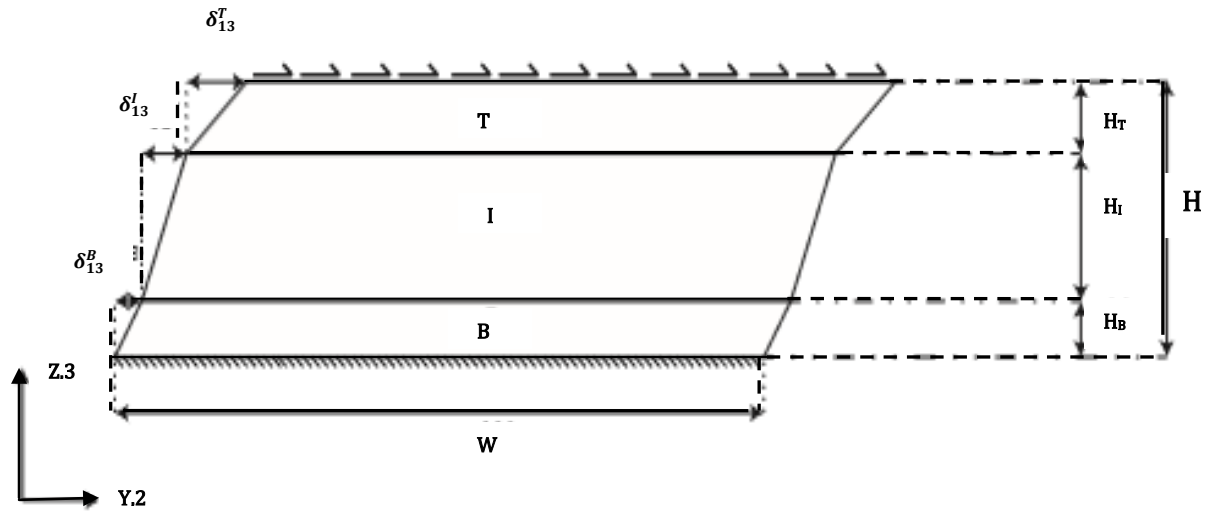

Figure 6: Assumed shear load for moduli G_{13} and G_{23}. The load is evenly distributed over the top sheet and fixed at the bottom.

Expressing the shear strain and displacement for all layers according to figure 3.17

$$\delta^{T}_{13} = \gamma^{T}_{13}.H^{T}, \delta^{I}_{13} = \gamma^{I}_{13}.H^{I}, \delta^{B}_{13} = \gamma^{B}_{13}.H^{B} \quad \textbf{(27)}$$

$$\delta_{13} = \delta_{13}^{T} + \delta_{13}^{I} + \delta_{13}^{B} = \gamma_{13}^{T}.H^{T} + \gamma_{13}^{I}.H^{I} + \gamma_{13}^{B}.H^{B} \quad \textbf{(28)}$$

Combining equations (27) and (28) give,

$$\gamma_{13} = \frac{\delta_{13}}{H} = \gamma_{13}^{T}.\frac{H^{T}}{H} + \gamma_{13}^{I}.\frac{H^{I}}{H} + \gamma_{13}^{B}.\frac{H^{B}}{H} \quad \textbf{(29)}$$

$$\gamma_{13} = \gamma_{13}^{T}.\alpha_{T} + \gamma_{13}^{I}.\alpha_{I} + \gamma_{13}^{B}.\alpha_{B} \quad \textbf{(30)}$$

Dividing all terms by τ_{13}gives,

$$\frac{\gamma_{13}}{\tau_{13}} = \gamma_{13}^{T}.\alpha_{T} + \frac{\gamma_{13}^{I}}{\tau_{13}}.\alpha_{I} + \gamma_{13}^{B}.\alpha_{B} \quad \textbf{(31)}$$

$$\frac{1}{G_{13}} = \frac{\alpha_{T}}{G_{13}^{T}} + \frac{\alpha_{I}}{G_{13}^{I}} + \frac{\alpha_{B}}{G_{13}^{B}} \quad \textbf{(32)}$$

Which gives the transformation for $G_{13}$and G_{23}:

$$G_{13} = \frac{1}{\frac{\alpha_{T}}{G_{13}^{T}} + \frac{\alpha_{I}}{G_{13}^{I}} + \frac{\alpha_{B}}{G_{13}^{B}}} \Longrightarrow G_{23} = \frac{1}{\frac{\alpha_{T}}{G_{23}^{T}} + \frac{\alpha_{I}}{G_{23}^{I}} + \frac{\alpha_{B}}{G_{23}^{B}}} \quad \textbf{(33)}$$

2.2.5 Poisson's ratios

Poisson's ratio is a measure of how much an object expands/contracts transversely during axial loading. A positive value Poisson's ratio gives contraction, which is the normal case, and a negative one gives expansion. The following procedure is used to obtain values for both transformation methods [1]. Assuming loading of P_{11}in direction1, each component will then have a displacement in direction 2 that can be expressed as:

$$\delta_{2}^{T} = -\nu_{12}^{T}.\varepsilon_{11}^{T}.W, \delta_{2}^{I} = -\nu_{12}^{I}.\varepsilon_{11}^{I}.W, \delta_{2}^{B} = -\nu_{12}^{B}.\varepsilon_{11}^{B}.W \quad \textbf{(34)}$$

The total displacement in direction 2 can be obtained by following expressions:

$$\delta_{2} = \alpha_{T}.\delta_{2}^{T} + \alpha_{I}.\delta_{2}^{I} + \alpha_{B}.\delta_{2}^{B} \quad \textbf{(35)}$$

Combining equation (41) with (40) and obtain following expressions:

$$\delta_{2} = -\alpha_{T}.\nu_{12}^{T}.\varepsilon_{11}.W - \alpha_{I}.\nu_{12}^{I}.\varepsilon_{11}.W - \alpha_{B}.\nu_{12}^{B}.\varepsilon_{11}.W \quad \textbf{(36)}$$

Total displacement for the 2-direction can also be expressed as $\delta_{2} = -\nu_{12}.\varepsilon_{11}.W$ which in turn gives:

$$-\nu_{12}.\varepsilon_{11}.W = -\alpha_T.\nu_{12}^T.\varepsilon_{11}^T.W - \alpha_I.\nu_{12}^I.\varepsilon_{11}^I.W - \alpha_B.\nu_{12}^B.\varepsilon_{11}^B.W \quad \textbf{(37)}$$

Divide both sides of equation (43) with $-\varepsilon_{11}.W$ gives'

$$\nu_{12} = -\alpha_T.\nu_{12}^T.\frac{\varepsilon_{11}^T}{\varepsilon_{11}} + \alpha_I.\nu_{12}^I.\frac{\varepsilon_{11}^I}{\varepsilon_{11}} + \alpha_B.\nu_{12}^B.\frac{\varepsilon_{11}^B}{\varepsilon_{11}} \quad \textbf{(38)}$$

Using the relation that all members suffer the same strain ε_{11}, i.e.:

$\varepsilon_{11}^T = \varepsilon_{11}^I = \varepsilon_{11}^B = \varepsilon_{11}$ putting into equation (38) gives,

$$\nu_{12} = \alpha_T.\nu_{12}^T + \alpha_I.\nu_{12}^I + \alpha_B.\nu_{12}^B \quad \textbf{(39)}$$

Considering ν_{13} instead under the stress σ_{11} which is defined as

$\nu_{13} = \frac{-\varepsilon_{33}}{\varepsilon_{11}}$. Displacement for 3-direction can be established as:

$$\delta_3^T = -\nu_{13}^T.\varepsilon_{11}^T.H_T,\ \delta_3^I = -\nu_{13}^I.\varepsilon_{11}^I.H_I,\ \delta_3^B = -\nu_{13}^B.\varepsilon_{11}^B.H_B \quad \textbf{(40)}$$

$$\delta_3 = \delta_3^T + \delta_3^I + \delta_3^B = -\nu_{13}^T\varepsilon_{11}^T H_T - \nu_{13}^I\varepsilon_{11}^I H_I - \nu_{13}^B\varepsilon_{11}^B H_B \quad \textbf{(41)}$$

Rewriting equation (41) by$\delta_3 = -\nu_{13}.\varepsilon_{11}.H$

$$-\nu_{13}.\varepsilon_{11}.H = -\nu_{13}^T\varepsilon_{11}^T H_T - \nu_{13}^I\varepsilon_{11}^I H_I - \nu_{13}^B\varepsilon_{11}^B H_B \quad \textbf{(42)}$$

Which is the same as,

$$\nu_{13} = -\nu_{13}^T\frac{\varepsilon_{11}^T H_T}{\varepsilon_{11}.H} - \nu_{13}^I\frac{\varepsilon_{11}^I I}{\varepsilon_{11}.H} - \nu_{13}^B\frac{\varepsilon_{11}^B H_B}{\varepsilon_{11}.H} \quad \textbf{(43)}$$

Step for deriving ν_{12} ,

$$\nu_{13} = \alpha_T.\nu_{13}^T + \alpha_I.\nu_{13}^I + \alpha_B.\nu_{13}^B \quad \textbf{(44)}$$

In the same manners,

$$\nu_{23} = \alpha_T.\nu_{23}^T + \alpha_I.\nu_{23}^I + \alpha_B.\nu_{23}^B \quad \textbf{(45)}$$

3. Results and discussions

3.1 Computer code in MATLAB™ to predict engineering constants

The selected mathematical formulations for engineering constants derived in the above **Section 2.1** are programmed in MATLAB™ code. Simulations for compression and flexural methods of the simply supported plate were selected. Three material properties were utilized

as initial engineering constant quantities for top-layer, core-layer, and bottom-layer consisting of Young's moduli, Poisson's ratios, and Shear moduli given in **Table 1**, **Table 2**, and **Table 3**, respectively. The seven material property sets with different parameters were chosen from [3]. Geometric and engineering properties for set of material properties given in [3] were utilized to simulate sandwich composite panels. Computer program developed in MATLAB^{TM} as shown in **Table 4** is executed to predict the effective engineering constants: Young's and Shear moduli, and Poisson's ratios for all the cases. Simulations were also carried out for the last two material sets that have a stiffer core compared to the face sheets, not a realistic case, and are chosen only on the basis to study and better understand the behaviour of the different transformations for possible improvements. To ensure that the chosen materials have a realistic behaviour, comparative checks of the load-displacement curve plots are drawn.

Table 4: MATLAB^{TM} Code for equivalent properties of sandwich panels

```
Clc;  close all;  clear all;  format('shortE');
 %% INPUT -TOP FACE SHEET (UPPER FLANGE);  ET=[23e9, 18e9, 20e9]; NU1T=[0.3, 0.3, 0.3];
 NUT=[NU1T, NU1T(1)/ET(1)*ET(2), NU1T(2)/ET(1)*ET(3), NU1T(3)/ET(2)*ET(3)];
 GT=[2.6e9, 600e6, 600e6]; 30 HT=0.0156; %% INTERMEDIATE-WEB (CORE); EI=[0, 0, 7e9]; NU1I=[0.3, 0.3, 0.3];
 NUI=[NU1I, NU1I(1)/EI(1)*EI(2), NU1I(2)/EI(1)*EI(3), NU1I(3)/EI(2)*EI(3)]; GI=[0.3333e9, 0.140625e9, 0.1046e9]; HI=0.1938;
 %% BOTTOM FACE SHEET (BOTTOM FLANGE);EB=[23e9, 18e9, 20e9];NU1B=[0.3, 0.3, 0.3];
NUB=[NU1B, NU1B(1)/EB(1)*EB(2), NU1B(2)/EB(1)*EB(3), NU1B(3)/EB(2)*EB(3)];
GB=[2.6e9, 600e6, 600e6]; HB=0.0156;  %% %% CHECK; EC=[ET;EI;EB]; NUC=[NUT;NUI;NUB];
 for i=1:length(EC);  if NUC(i,1) > sqrt(EC(i,1)/EC(i,2));  disp('ERROR not valid material properties'); i ;  end
 if NUC(i,2) > sqrt(EC(i,1)/EC(i,3)); disp('ERROR not valid material properties'); i ; end
 if NUC(i,3) > sqrt(EC(i,3)/EC(i,2)); disp('ERROR not valid material properties'); i ; end
 if 1−NUC(i,1)*NUC(i,4)−NUC(i,3)*NUC(i,6)−NUC(i,2)*NUC(i,5)− 2*NUC(i,4)*NUC(i,6)*NUC(i,2) < 0;
 disp('ERROR not valid material properties'); i ; end ;end% CHECK OF ASSUMPTIONS
 H=HT+HI+HB; xNx=(−EB(1)*HB^2+2*EB(1)*H*HB+ET(1)*HT^2+EI(1)*H*HI)/(2*(EB(1)*A-10;
HB+EI(1)*HI+ET(1)*HT));  xNy=(−EB(2)*HB^2+2*EB(2)*H*HB+ET(2)*HT^2+EI(2)*H*HI)/(2*(EB(2)*...
HB+EI(2)*HI+ET(2)*HT));74 if xNx>HT+HI | xNx<HT; 75 disp('ERROR neutral axis is not in the core in x−direction');
End; if xNy>HT+HI | xNy<HT ; disp('ERROR neutral axis is not in the core in y−direction'); end;
 %% CONTROL OF RELATIONS BETWEEN SHEAR VALUES FOR ACCURATE TRANSFORMATION
for e=2:3;diffG=max([GT(e),GI(e),GB(e)])/min([GT(e),GI(e),GB(e)]); 83 if diffG≥1e3;
disp('WARNING! LARGE DIFFERENCE IN SHEAR MODULUS. THIS MAY LEAD TO INACCURATE RESULT'); end; end;%%
ALGORITHM; at=HT/H; ai=HI/H; ab=HB/H; E11=at*ET(1)+ai*EI(1)+ab*EB(1);E22=at*ET(2)+ai*EI(2)+ab*EB(2);
 E33=1/(at/ET(3)+ai/EI(3)+ab/EB(3));
 Eeq11=(12*ET(1)*(HT^3/12 + (HT*(− EB(1)*HB^2 + 2*EB(1)*H*HB + ET(1)*HT^2 + ... EI(1)*H*HI)^2)/(4*(EB(1)*HB + EI(1)*HI +
ET(1)*HT)^2)))/H^3 + (12*EB(1)*(HB^3/12 + ... HB*(H − (− EB(1)*HB^2 + 2*EB(1)*H*HB + ET(1)*HT^2 +
EI(1)*H*HI)/(2*(EB(1)*HB + EI(1)*HI ... + ET(1)*HT)))^2))/H^3 + (12*EI(1)*(HI^3/12 + HI*(HI/2 + HT/2 − (− EB(1)*HB^2 + ...
2*EB(1)*H*HB + ET(1)*HT^2 + EI(1)*H*HI)/(2*(EB(1)*HB + EI(1)*HI + ET(1)*HT)))^2))/H^3;
Eeq22=(12*ET(2)*(HT^3/12 + (HT*(− EB(2)*HB^2 + 2*EB(2)*H*HB + ET(2)*HT^2 + ... EI(2)*H*HI)^2)/(4*(EB(2)*HB + EI(2)*HI +
ET(2)*HT)^2)))/H^3 + (12*EB(2)*(HB^3/12 + ... HB*(H − (− EB(2)*HB^2 + 2*EB(2)*H*HB + ET(2)*HT^2 +
```

```
EI(2)*H*HI)/(2*(EB(2)*HB + EI(2)*HI ... + ET(2)*HT)))^2))/H^3 + (12*EI(2)*(HI^3/12 + HI*(HI/2 + HT/2 − (− EB(2)*HB^2 + ...
2*EB(2)*H*HB + ET(2)*HT^2 + EI(2)*H*HI)/(2*(EB(2)*HB + EI(2)*HI + ET(2)*HT)))^2))/H^3;
G12=at*GT(1)+ai*GI(1)+ab*GB(1);G21=G12;G13=1/(at/GT(2)+ai/GI(2)+ab/GB(2));G31=G13; G23=1/(at/GT(3)+ai/GI(3)+ab/GB(3));
G32=G23; test=at*GT(3)+ai*GI(3)+ab*GB(3);
 NU12=at*NUT(1)+ai*NUI(1)+ab*NUB(1); NU13=at*NUT(2)+ai*NUI(2)+ab*NUB(2); NU23=at*NUT(3)+ai*NUI(3)+ab*NUB(3);
KINA_EG=[E11,E22,E33,G12,G13,G23]';  EQ=[Eeq11, Eeq22, E33, G12, G13, G23]';
NUU=[NU12, NU13, NU23]';  %% OUTPUT  KINA_EG EQ  format('short'); NUU
```

3.2 Results and discussions

Simulations were performed utilizing axial-compression and flexural methods for the input data given in tabular forms below for Top-, Core-, and Bottom-layer in rows: 3-5 taken from [3]. The simulation generated data quantities are also presented for comparison against the corresponding engineering constant quantities in rows: 11-12 of the same tables. It can be seen that elastic, shear moduli, and Poisson's 5 sets of realistic materials under corresponding columns match well in **Table 5**, **Table 6**, **Table 7**, **Table 8**, and **Table 9**. Similarly, last two unrealistic material data sets that have a stiffer core compared to the face sheets, the un-realistic cases confirm transformations are shown in **Table 10**, and **Table 11**. In both the realistic and un-realistic cases, generated data exhibit good correlation. The data quantities illustrated are according to the expectation and no outlier (abrupt change) can be seen. Better overall correlation is achieved according to the transformation results based on constant flexural rigidity and axially loaded deflection. Close correlation can be seen for flexural method in all sets except for set 7 where the core (as a web) is much stiffer compared to the sheets (as flanges). Intra comparison of the flexural and compression transformation gives that flexural results are more accurate result than the axial-compressive ones. Even though the result differs substantially from the reference one in some cases. It can be seen that the elastic, shear moduli, and Poisson's ratios quantities depicted in the tables under corresponding columns the input data quantities.

Table 5: Initial values of material parameters set 1

Given material stiffness parameters [Pa]										
Layer	E_{xx}	E_{yy}	E_{zz}	V_{xx}	V_{xx}	V_{zz}	G_{12}	G_{13}	G_{23}	h(m)
TOP	16.6e9	9.58e9	9.58e9	0.31	0.31	0.29	5.12e9	4.87e9	3.72e9	0.03
CORE	6.55e9	0.17e9	5.52e9	0.33	0.33	0.1	0.483e9	5.45e9	0.345e9	0.19
BOT	12.4e9	6.21e9	6.21e9	0.31	.31	0.29	3.6e9	3.38e9	2.41e9	0.05
Simulation generated equivalent material stiffness parameters [Pa]										
Model: three-point beam flexural method										
E_{xx}		E_{yy}	E_{zz}	V_{xx}	V_{xx}	V_{zz}	G_{12}	G_{13}	G_{23}	
15.4e9		6.77e9	5.93e9	0.324	0.324	0.156	1.58e9	4.84e9	0.466e9	

Model: axial-compressive								
E_{xx}	**E_{yy}**	**E_{zz}**	**V_{xx}**	**V_{xx}**	**V_{zz}**	**G_{12}**	**G_{13}**	**G_{23}**
8.75e9	2.33e9	5.93e9	0.324	0.324	0.156	0.583e9	5.84e9	0.466e9

Table 6: Initial values of material parameters set 2

Given material stiffness parameters [Pa]										
E_{xx}	E_{yy}	E_{yy}	E_{zz}	V_{xx}	V_{xx}	V_{zz}	G_{12}	G_{13}	G_{23}	h(m)
TOP	210.6e9	210.6e9	210.6e9	0.3	0.3	0.3	80.7e9	80.7e9	80.7e9	0.03
CORE	0.36e9	0.36e9	0.36e9	0.08	0.08	0.08	0.097e9	0.097e9	0.097e9	0.19
BOT	210.4e9	210.4e9	210.4e9	0.3	.3	0.3	80.7e9	80.7e9	80.7e9	0.05
Simulation generated equivalent material stiffness parameters [Pa]										
Model: three-point beam flexural method										
E_{xx}		E_{yy}	E_{zz}	V_{xx}	V_{xx}	V_{zz}	G_{12}	G_{13}	G_{23}	
178e9		178e9	0.511e9	0.145	0.145	0.145	24.0e9	0.138e9	0.138e9	
Model: axial-compressive										
Model	**E_{xx}**	**E_{yy}**	**E_{zz}**	**V_{xx}**	**V_{xx}**	**V_{zz}**	**G_{12}**	**G_{13}**	**G_{23}**	
62.5e9		62.5e9	0.511e9	0.145	0.145	0.145	24.0e9	0.138e9	0.138e9	

Table 7: Initial values of material parameters set 3

Given material stiffness parameters [Pa]										
Layer	E_{xx}	E_{yy}	E_{zz}	V_{xx}	V_{xx}	V_{zz}	G_{12}	G_{13}	G_{23}	h(m)
TOP	100.6e9	20.e9	20.e9	0.2	0.3	0.1	5e9	10e9	7e9	0.03
CORE	2e9	0.2e9	0.2e9	0.1	0.2	0.1	0.1e9	0.5e9	0.3e9	0.19
BOT	20.4e9	100.4e9	100.4e9	0.3	.31	0.29	10.e9	5e9	7e9	0.05
Simulation generated equivalent material stiffness parameters [Pa]										
Model: three-point flexural										
E_{xx}		E_{yy}	E_{zz}	V_{xx}	V_{xx}	V_{zz}	G_{12}	G_{13}	G_{23}	
34.8e9		26.4e9	6.56e9	0.148	0.232	0.135	2.48e9	0.68e9	0.418e9	
Model: axial-compressive										
E_{xx}		E_{yy}	E_{zz}	V_{xx}	V_{xx}	V_{zz}	G_{12}	G_{13}	G_{23}	
16.2e9		20.9e9	6.56e9	0.148	0.232	0.135	2.48e9	0.68e9	0.418e9	

Table 8: Initial values of material parameters set 4

Given material stiffness parameters [Pa]										
Layer	E_{xx}	E_{yy}	E_{zz}	V_{xx}	V_{xx}	V_{zz}	G_{12}	G_{13}	G_{23}	h(m)
TOP	2000.6e9	1000e9	500.e9	0.05	0.06	0.05	200e9	100e9	400e9	0.03
CORE	0.02e9	0.04e9	0.5e9	0.1	0.1	0.05	0.5e9	0.9e9	01e9	0.19
BOT	400e9	200e9	40e9	0.1	.1	0.29	50.e9	53e9	71e9	0.05
Simulation generated equivalent material stiffness parameters [Pa]										
Model: three-point flexural										
E_{xx}		E_{yy}	E_{zz}	V_{xx}	V_{xx}	V_{zz}	G_{12}	G_{13}	G_{23}	
673e9		337e9	0.708e9	0.094	0.096	0.078	31.8e9	1.27e9	1.42e9	
Model: axial-compressive										
E_{xx}		E_{yy}	E_{zz}	V_{xx}	V_{xx}	V_{zz}	G_{12}	G_{13}	G_{23}	
296e9		148e9	0.708e9	0.094	0.096	0.078	31.8e9	1.27e9	1.42e9	

Table 9: Initial values of material parameters set 5

Given material stiffness parameters [Pa]										
Layer	E_{xx}	E_{yy}	E_{zz}	V_{xx}	V_{xx}	V_{zz}	G_{12}	G_{13}	G_{23}	h(m)
TOP	206e9	2e9	50.e9	0.15	0.26	0.12	5e9	3e9	1e9	0.03
CORE	0.02e9	0.046e9	0.2e9	0.13	0.22	0.09	0.4e9	0.09e9	0.1e9	0.19
BOT	15e9	40e9	1e9	0.15	.11	0.15	2.e9	3e9	24e9	0.05
Simulation generated equivalent material stiffness parameters [Pa]										
Model: three-point flexural										
E_{xx}	E_{yy}	E_{zz}	V_{xx}	V_{xx}	V_{zz}	G_{12}	G_{13}	G_{23}		
15.0e9	3.69e9	0.270e9	0.136	0.201	0.104	1218e9	0.126e9	0.140e9		
Model: axial-compressive										
E_{xx}	**E_{yy}**	**E_{zz}**	**V_{xx}**	**V_{xx}**	**V_{zz}**	**G_{12}**	**G_{13}**	**G_{23}**		
5.01e9	7.66e9	0.270e9	0.136	0.201	0.104	1.21e9	0.26e9	0.140e9		

Table 10: Initial values of material parameters set 6

Given material stiffness parameters [Pa]										
Layer	E_{xx}	E_{yy}	E_{zz}	V_{xx}	V_{xx}	V_{zz}	G_{12}	G_{13}	G_{23}	h(m)
TOP	2e9	5e9	10e9	0.2	0.1	0.3	5e9	0.3e9	0.1e9	0.03
CORE	200e9	100e9	300e9	0.23	0.12	0.3	10e9	0.5e9	2e9	0.19
BOT	10e9	20e9	2e9	0.12	.15	0.2	5e9	1e9	5e9	0.05
Simulation generated equivalent material stiffness parameters [Pa]										
Model: three-point flexural										
E_{xx}	E_{yy}	E_{zz}	V_{xx}	V_{xx}	V_{zz}	G_{12}	G_{13}	G_{23}		
91.8e9	57.3e9	7.58e9	0.206	0.123	0.282	8.02e9	0.509e9	0.667e9		
Model: axial-compressive										
E_{xx}	E_{yy}	E_{zz}	V_{xx}	V_{xx}	V_{zz}	G_{12}	G_{13}	G_{23}		
142e9	74.6e9	7.58e9	0.206	0.123	0.282	8.02e9	0.509e9	0.667e9		

Table 11: Initial values of material parameters set 7

Given material stiffness parameters [Pa]										
Layer	E_{xx}	E_{yy}	E_{zz}	V_{xx}	V_{xx}	V_{zz}	G_{12}	G_{13}	G_{23}	h(m)
TOP	0.2e9	5e9	0.3e9	0.12	0.11	0.23	0.05e9	0.03e9	0.01e9	0.03
CORE	200e9	1000e9	600e9	0.15	0.12	0.23	100e9	6e9	10e9	0.19
BOT	1e9	2e9	22e9	0.17	.14	0.15	0.5e9	10e9	1e9	0.05
Simulation generated equivalent material stiffness parameters [Pa]										
Model: three-point flexural										
E_{xx}	E_{yy}	E_{zz}	V_{xx}	V_{xx}	V_{zz}	G_{12}	G_{13}	G_{23}		
84.9e9	423e9	2.63e9	0.150	0.193	0.215	70.5e9	0.260e9	0.088e9		
Model: axial-compressive										
E_{xx}	E_{yy}	E_{zz}	V_{xx}	V_{xx}	V_{zz}	G_{12}	G_{13}	G_{23}		
141e9	705e9	2.63e9	0.150	0.193	0.215	70.5e9	0.260e9	0.088e9		

3.3 Verification of the analysis

Since sandwich plate may work like a plate resting on two supports as an upper flange for the global beam frame systems that can compliment verification and establish a reliable evaluation of the two different transformation methods. Likewise, deflection between two

girders is close to pure bending which favour the transformation based on constant flexural rigidity. Furthermore, loading in the other direction is a combination of bending and axial loading that does not make it apparent which of the two transformation methods that should be favoured. Thus, transformation method verified by comparison of the deflection is selected.

The simulation generated data results by the axial-compression and flexural methods, the deflection quantities U_3 are plotted against reference [3] quantities in x-directions. Comparisons of the deflection quantities by axial-compressive and flexural methods against referred method for input data set 1 and set 2 are plotted in **Figure 7** and **Figure 8** respectively. Comparison of flexural and referred curves illustrate slight different but similar downward trend. Nonetheless, it can be seen that the deflection curve representing axial-compressive quantities show much more deflection when compared to the flexural and referred curves. This means a situation may have occurred where extensional moduli E_{11} and E_{22} for a certain allowed deflection were not stiff enough, and result in a larger deflection (outlier).

Comparisons of the deflection quantities by axial-compressive and flexural methods against referred method for input data set 3, 4, and 5 are plotted **Figure 9**, **Figure 10**, and **Figure 11**, respectively. Comparison of flexural and referred curves illustrate slight different but similar downward trend in **Figure 9** and **Figure 10**, however the curves swap their positions in **Figure 11** where referred curve exhibits relatively larger deflection quantities than flexural ones. Nonetheless, the deflection curve representing axial-compressive method curve shows larger deflection compared to the flexural and referred curves. The comparisons confirmed that weaker extensional moduli E_{11} and E_{22} resulted in a larger deflection (outlier). The simulated deflection is a combination of flexural and shear deflection. However, deflection caused by flexural usually contributes much more to the total deflection, compared to shear deflection. Comparisons of the deflection quantities by axial-compressive and flexural methods against referred method for input data set 6 and 7 are plotted **Figure 12**, **Figure 13**, respectively. Comparison of axial-compressive, flexural, and referred curves illustrate slight difference in quantities but similar downward trend though flexural and referred curves swap their positions in **Figure 12**. A reverse pattern can be observed in **Figure 13** where flexural method curve exhibits larger deflection quantities than the referred and axial-compressive ones. Furthermore, the deflection curve representing referred method shows smaller deflection compared to the flexural and referred curves. The comparisons confirmed that

stronger extensional moduli E_{11} and E_{22} resulted in a smaller deflection. The last material set gives a bad correlation. This may be a result from the large difference between the layers for material parameters G_{13} and G_{23}. The equations used for the transformation have very similar properties as an equation used to calculate. This means that a very small value affects the transformed shear modulus to a large extent.

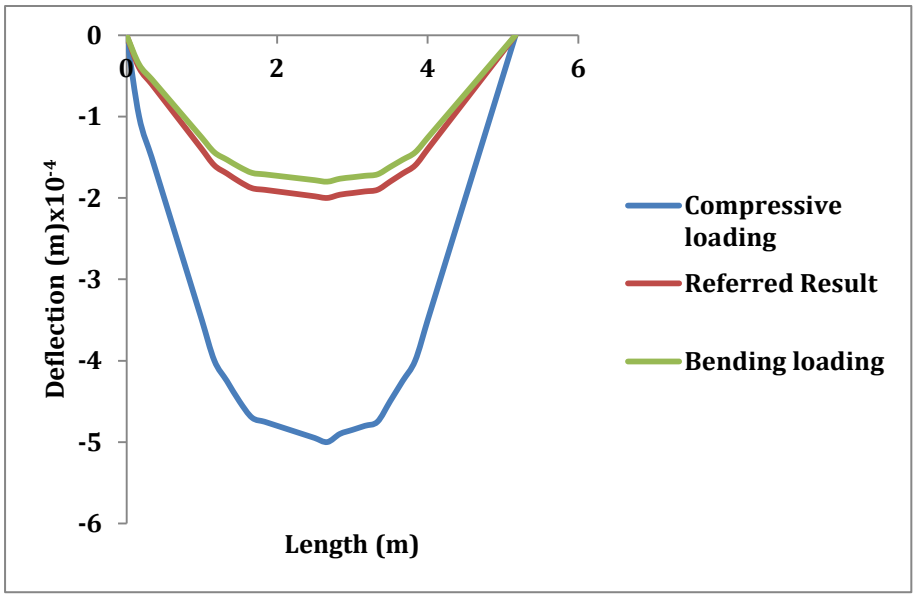

Figure 7: Deflection U3 along x-direction for parameter set 1.

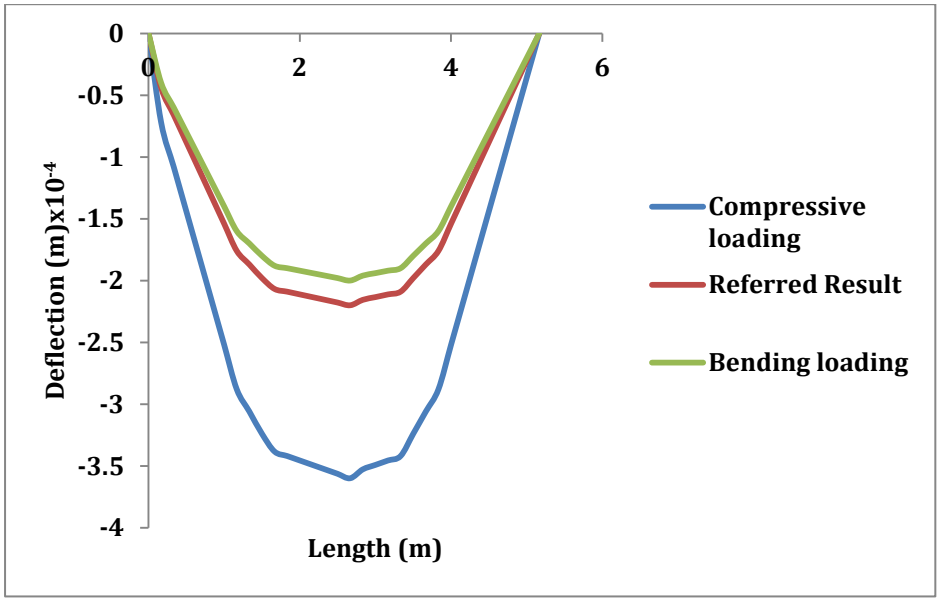

Figure 8: Deflection U3 along x-direction for parameter set 2.

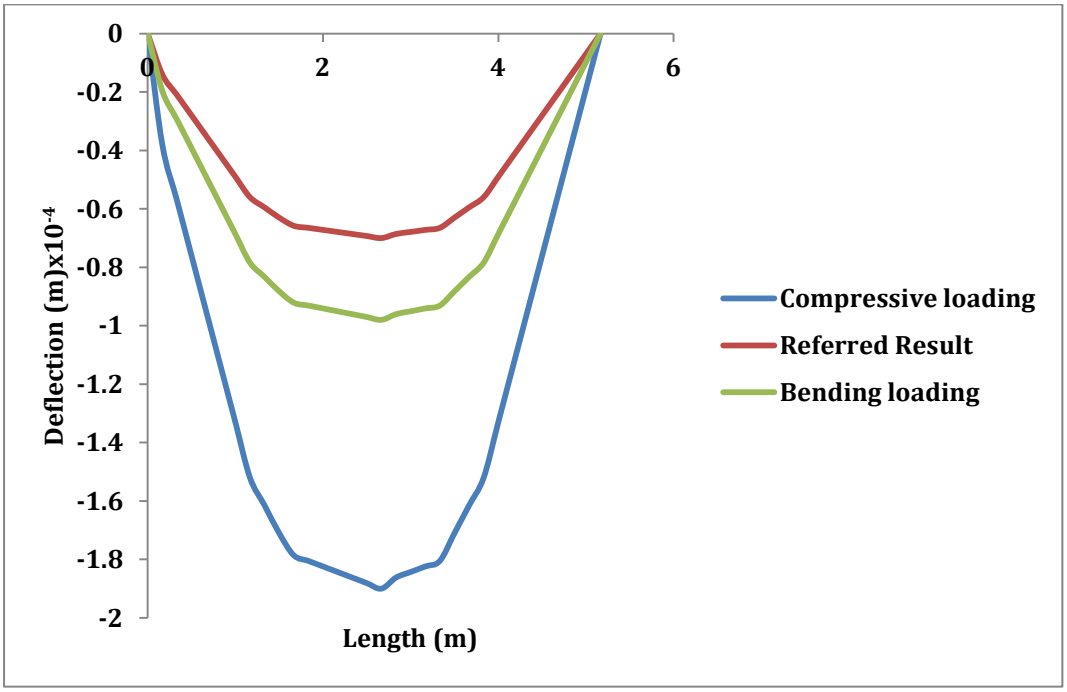

Figure 9: Deflection U3 along x-direction for parameter set 3.

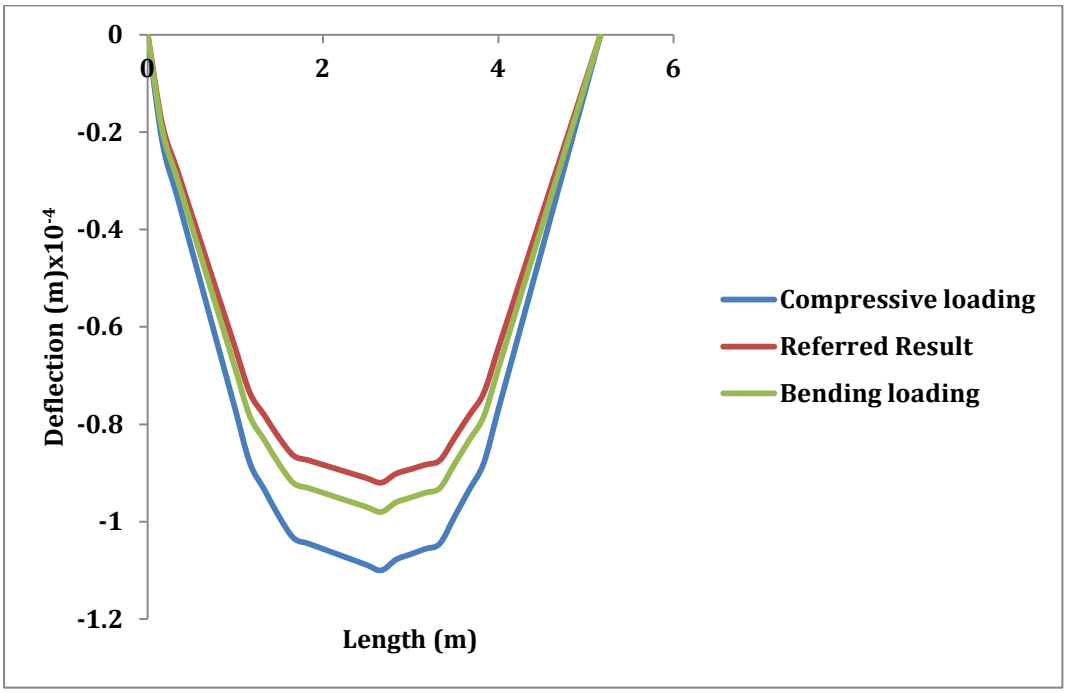

Figure 10: Deflection U3 along x-direction for parameter set 4.

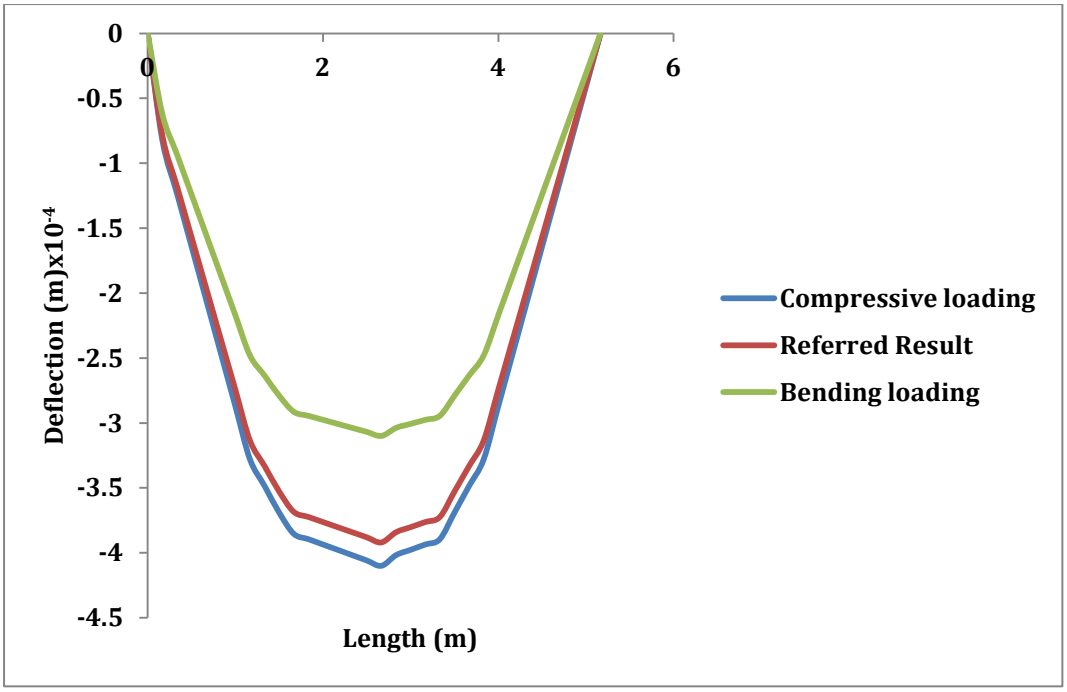

Figure 11: Deflection U3 along x-direction for parameter set 5.

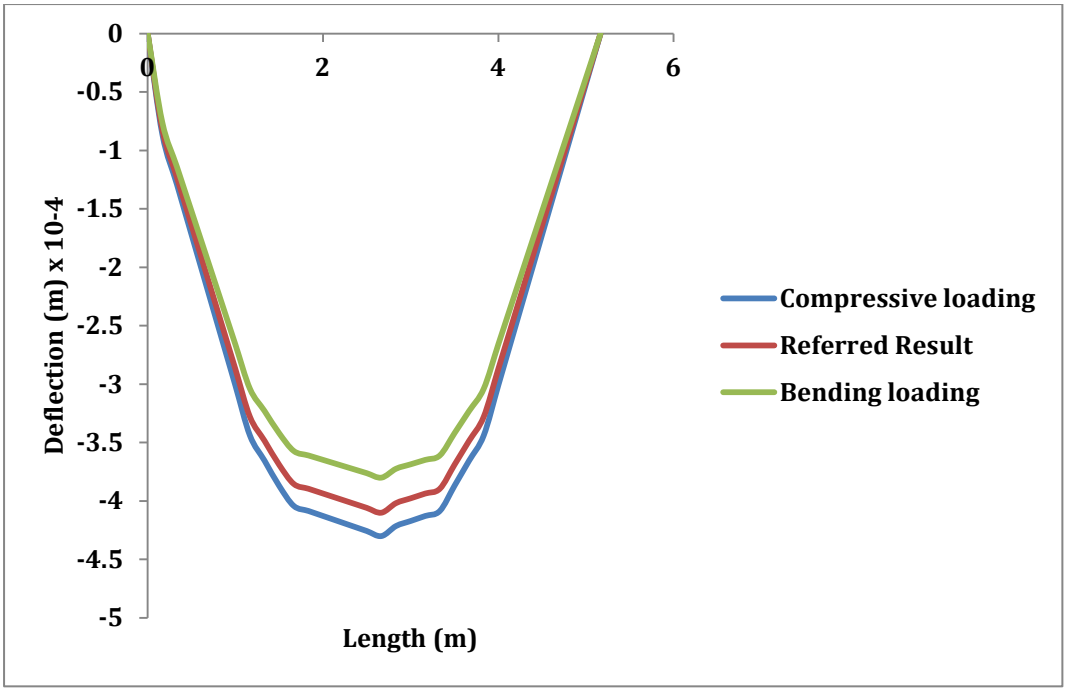

Figure 12: Deflection U3 along x-direction for parameter set 6.

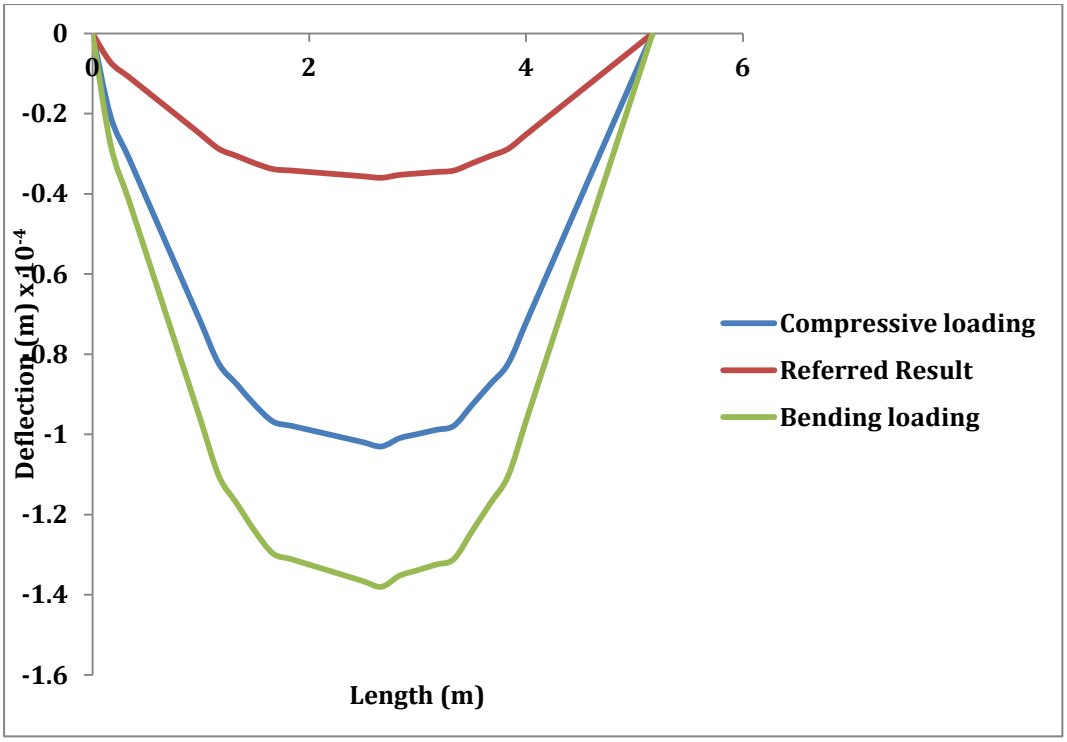

Figure 13: Deflection U3 along x-direction for parameter set 7.

It was observed that the elastic, shear moduli, and Poisson's ratios quantities agree well with referred quantities depicted in the tables. The transformation methods are normally verified by comparison of the deflection. Since deflection is a combination of bending and shear, and contributes much more to the total deflection compared to shear. Furthermore, flexural method is preferred for the optimization purposes in practice despite results might differ to some extent.

The graphical visualisation of computer simulations generated data by axial-compression and flexural methods for both the realistic and un-realistic data cases exhibit similar trends. The data quantities illustrated are according to the expectation. Close correlation is observed for flexural method in all sets except for set 7 where the core (web) is much stiffer compared to the sheets (flanges). Intra comparison of the flexural and compression transformation gives that flexural results are more accurate result than the axial-compressive ones. Even though the result differs substantially from the reference one in some cases.

4. Conclusions

Analytical and simulation analyses of sandwich composite panels were performed to approximate effective engineering constants using axial-compressive and flexural bending

techniques. All relationships have been established for a certain thickness of the sandwich plate and stiffness. Selected results were compared to the data results available in literature and found to be within the acceptable agreement up to (±8%) deviations. Based on comparison the results, the following conclusions are extracted:

1. Overall the transformation based on constant flexural rigidity method seems to have better correlation, more stable, and not varying as much between the different parameter sets than the other axial deformation and referred methods.
2. The stiffness (E_{11}) affects the longitudinal deflection, the other direction (E_{22}) pure bending, it is much more viable to increase E_{22} instead of E_{11} to decrease the deflection, and vice versa for a case with opposite stiffness division
3. Overcapacity of shear stiffness G_{13} and G_{23} utilizes the material until linear strain limits, and relation between G_{23} and E_{22} provides linear strain.
4. A change in the Poisson's ratio (stiffness ratio) could greatly affect the strain over the thickness structure.
5. The axial-compression method gives unacceptable and bad correlation for some parameter sets, as the real case is combination depends on the direction.

Analysis can be useful not only to approximate engineering properties but also to accommodate stiffness in different directions for orthotropic materials by changing the fibre direction, adding ribs, truss, or other stiffness altering features.

References

[1] Zhou, Aixi. Stiffness and strength of fibre reinforce polymer composite bridge deck system 2002; In: pp. 78– 83.

[2] N. Gupta, Characterization of syntactic foams and their sandwich composites: modelling and experimental approaches, Dissertation Thesis, Louisiana State University and Agricultural and Mechanical College, USA, 2003.

[3] ISAK A B VIKTOR. Evaluation and optimization of orthotropic sandwich plate systems with regard to global deflection: finite element simulation and analytical evaluation. MSc Thesis, Department of Civil and Environmental Engineering Division of Structural Engineering Chalmers University Göteborg, Sweden 2012.

[4] Konka H. P., Wahab M. A. K. On Mechanical Properties of Composite Sandwich Structures With Embedded Piezoelectric Fiber Composite Sensors. Journal of Engineering Materials and Technology 2012;134:1-11.

[5] Foo C. C., Chai G. B., and Seah L. K.Mechanical properties of Nomex material and Nomex honeycomb structure. Compos Struct 2007;80:588-594.

[6] Abbadi A., Koutsawa Y., Carmasol A., Belouettar S., and Azari Z. Experimental and numerical characterization of honeycomb sandwich composite panels. Simulation Modelling Practice and Theory 2009;17:1533-1547.

[7] ASTM D3039/D3039M-14. Standard test method for tensile properties of polymer matrix composite materials. West Conshohocken, PA: ASTM International, 2014.

[8] ASTM C393/C393M-16. Standard test method for core shear properties of sandwich constructions by beam flexure. West Conshohocken, PA: ASTM International, 2016.

[9] ASTM D3410/D3410M-16. Standard test method for axial-compressive properties of polymer matrix composite materials with unsupported gage section by shear loading. West Conshohocken, PA: ASTM International, 2016.

[10] ASTM D3518/D3518M-13. Standard test method for in-plane shear response of polymer matrix composite materials by tensile test of a 45 laminate. West Conshohocken, PA: ASTM International, 2013.

[11] Gupta N, Ye R, Porfiri M. Comparison of tensile and axial-compressive characteristics of vinyl/glass micro-balloon syntactic foams. Compos Part B-Eng 2010;41:236–245.

[12] Côté F., Deshpande V. S., Fleck N. A., and Evans A. G. The axial-compressive and shear of corrugated and diamond lattice materials 2006. Int J Sol Struct 2006; 6220-6242.

[13] Yan LL, Yu B, Han B, et al. Axial-compressive strength and energy absorption of sandwich panels with Al foam-filled corrugated cores. Compos Sci Technol 2013; 86: 142–148.

[14] Yan LL, Han B, Yu B, et al. Three-point flexural of sandwich beams with aluminium foam-filled corrugated cores. Mater Des 2014; 60: 510–519.

[15] Gryzagoridis, J.; Oliver, G.; Findeis, D. On the equivalent flexural rigidity of sandwich composite panels. Insight-Non-Destr. Test. Cond. Monit. 2015;57:140–143.

[16] Juntikka R, Hallstrom S. Shear characterization of sandwich core materials using four-point flexural. J Sandwich Struct Mater 2007;9(1):67–94.

[17] Mostafa A, Shankar K, Morozov EV. Insight into the shear behaviour of composite sandwich panels with foam core. Mater Design 2013;50:92–101.

[18] Salleh Z, Islam M, Ku H. Study on Axial-compressive Properties of Syntactic Foams for Marine Applications. J Multifunctional Compos 2014;2: 21–27.

[19] Nasirzadeh R, Sabet AR. Study of foam density variations in composite sandwich panels under high velocity impact loading. Int J Impact Eng 2014;63:129–139.

[20] Rajaneesh A, Sridhar I, Rajendran S. Relative performance of metal and polymeric foam sandwich plates under low velocity impact. Int J Impact Eng 2014;65:126–136.

[21] Fathi A, Wolff-Fabris F, Altsta¨dt V, Ga¨tzi R. An investigation on the flexural properties of balsa and polymer foam core sandwich structures: influence of core type and contour finishing options. J Sandwich Struct Mater 2013;15(5):487–508.

[22] Cheol-Won Kong, Gi-Won Nam, Young-Soon Jang & Yeong-Moo Yi. Experimental strength of composite sandwich panels with cores made of aluminium honeycomb and foam, Advanced Compos Mater 2014;23:143-52.

[23] Karaduman Y and Onal L. Flexural behaviour of commingled polyprop nonwoven fabric reinforced sandwich composites. Compos Part B Eng 2016;93:12–25.

[24] Kaboglu C, Pimenta S, Morris A, Dear JP. The effect of different types of core material on the flexural behaviour of sandwich composites for wind turbine blades. J Therm Eng 2017;3(2):1102–1109.

[25] Shi H, Liu W and Fang H. Damage characteristics analysis of GFRP-balsa sandwich beams under four-point fatigue flexural. Compos Part A Appl Sci Manuf 2018;109:564–577.

[26] Li G, Fang Y, Hao P, et al. Three-point flexural deflection and failure mechanism map of sandwich beams with second-order hierarchical corrugated truss core. J Sandwich Struct Mater 2017;19: 83–107.

[27] Zhou J, Guan ZW and Cantwell WJ. Scaling effects in the mechanical response of sandwich structures based on corrugated composite cores. Compos Part B Eng 2016;93:88–96.

[28] Kılıc¸ aslan C, Odacı _IK and Gu¨ den M. Single- and double-layer aluminium corrugated core sandwiches under quasi-static and dynamic loadings. J Sandwich Struct Mater 2016;18: 667–692.

[29] Osei-Antwi M, de Castro J, Vassilopoulos AP, et al. Modelling of axial and shear stresses in multilayer sandwich beams with stiff core layers. Compos Struct 2014;116:453–460.

[30] Yu Y, Ying L, Hou W-B, et al. Failure analysis of adhesively bonded steel corrugated sandwich structures under three-point flexural. Compos Struct 2018;184:256–268.

[31] Han B, Qin K, Yu B, et al. Honeycomb–corrugation hybrid as a novel sandwich core for significantly enhanced axial-compressive performance. Mater Des 2016;93:271–282.

[32] Kamareh F, Farrokhabadi A and Rahimi G. Experimental and numerical investigation of skin/lattice stiffener debonding growth in composite panels under flexural loading. Eng Fract Mech 2018;190:471–490.

[33] Khelifa M and Celzard A. Numerical analysis of flexural strengthening of timber beams reinforced with CFRP strips. Compos Struct 2014;111:393–400.

[34] Feli S and Jafari SS. Analytical investigation of perforation of aluminium–foam sandwich panels under ballistic impact. Modares Mech Eng 2013;13:52–59.

[35] Alavi, Nia A and Kazemi M. Analytical study of high velocity impact on sandwich panels with foam core and Al face-sheets. Modares Mech Eng 2015;15:231–239.

[36] Cheng Q, Lee H, Lu C. A numerical analysis approach for evaluating elastic constants of sandwich structures with various cores. Compos Struct 2006;74:226–236.

[37] Ziya MS, Khoda, Rahmi H, Vahedi K, et al. Experimental and numerical investigation of a blunt rigid projectile penetrating into a sandwich panel having aluminium foam core. Modares Mech Eng 2013;13:1–13.

[38] Su B, Zhou Z, Zhang J, et al. A numerical study on the impact behaviour of foam-cored cylindrical sandwich shells subjected to normal/oblique impact. Latin Am J Solids Struct 2015;12: 2045–2060.

[39] He W, Liu J, Tao B, et al. Experimental and numerical research on the low velocity impact behaviour of hybrid corrugated core sandwich structures. Compos Struct 2016;158:30–43.

[40] [8] S. Heimbs, "Virtual testing of sandwich core structures using dynamic finite element simulations," Computational Materials Science, vol. 45, pp. 205-216, 2009.

[41] Bartolozzi G., Pierini M., Orrenius U., and Baldanzini N. An equivalent material formulation for sinusoidal corrugated cores of structural sandwich panels, Composite Structures 2013;100:173-185.

[42] Bartolozzi G., Baldanzini N., and Pierini M. Equivalent properties for corrugated cores of sandwich structures: A general analytical method, Compos Struct 2014;108:736-746.